THE ASTROPHYSICAL JOURNAL, 499:L215–L218, 1998 June 1

SOLAR WIND CONSEQUENCES OF A CORONAL HOLE DENSITY PROFILE: SPARTAN 201-03 CORONAGRAPH AND *ULYSSES* OBSERVATIONS FROM 1.15 $R_\odot$ TO 4 AU

MADHULIKA GUHATHAKURTA[1] AND RICHARD FISHER
NASA Goddard Space Flight Center, Code 682, Greenbelt, MD 20771

Received 1998 January 23; accepted 1998 March 24; published 1998 May 22

ABSTRACT

Spartan 201 is a small shuttle-launched and -retrieved satellite, whose mission is to study the origins of the solar wind. It carries on board two instruments, the Ultraviolet Coronal Spectrometer and the White-Light Coronagraph. The third mission of the Spartan 201 (1995 September 7–10) spacecraft was to provide a solar context for the in situ particles and fields measurements during the north polar passage of the *Ulysses* spacecraft. In this Letter, we characterize the physical conditions of the north polar coronal hole as derived from white-light coronal observations by the Spartan 201-03 White-Light Coronagraph, the ground-based K coronameter in Mauna Loa, Hawaii, and *Ulysses* observations of in situ particles and their velocity. For the first time, we are able to combine in situ and path-integrated measurements in a coronal hole, to yield a consistent electron density (N) profile from the Sun to the Earth and the outer heliosphere. By using the value of N measured by *Ulysses* (1.8–4 AU), we are able to determine the actual value of N and *not just an upper limit* in the polar coronal hole, near the Sun. The current N profile suggests that the acceleration of the fast solar wind in a coronal hole is complete by 10–15 $R_\odot$, much closer to the Sun than had been previously expected.

Subject headings: solar wind — Sun: corona

1. INTRODUCTION

The importance of white-light density constraints in solar wind modeling has been established recently by several studies (Guhathakurta & Fisher 1996; Habbal et al. 1995; Ko et al. 1997). All solar wind modeling requires the knowledge of the density and temperature at the base of the corona as boundary conditions. What is also required is the knowledge of the magnetic field geometry. The expansion factor is often used as a parameter in one-dimensional models to represent the magnetic field geometry of the flow/flux tubes. White-light polarized brightness observations can provide both the density (Guhathakurta, Holzer, & MacQueen 1996, hereafter GHM96; Fisher & Guhathakurta 1995, hereafter FG95) and the magnetic field geometry (Guhathakurta & Holzer 1994) of flow tubes and large-scale structures. Indirect inference of hydrostatic temperature can also be obtained from the electron density in the solar corona (Guhathakurta & Fisher 1995), and such a profile matches quite well the estimated "freeze-in" temperature in the coronal hole from the measured solar wind ionic charge states (Ko et al. 1997).

Polarized brightness (pB) observed in the corona is the result of the integration of the density over the line of sight of the observer. Thus, in the past, the electron density inside a coronal hole was always estimated to be an upper limit to the true electron density in the corona. For the first time, simultaneous observations of the pB of the north polar solar corona close to the Sun, and particles and velocity observations by *Ulysses* beyond 1 AU, were made during the third flight of Spartan 201 and the north polar passage of the *Ulysses* spacecraft. Combining the *Ulysses* in situ observations of N with the inferred electron density from the Spartan 201-03 White-Light Coronagraph (WLC), we derive an electron density profile starting at the Sun and extending to the outer heliosphere. We also show in this Letter how these data can be used to put empirical constraints on flow velocity and effective temperature, especially near the Sun.

2. OBSERVATIONS AND ANALYSIS

The goal of the third mission of the Spartan 201 spacecraft was to provide a spatial context for the in situ particles and fields measurements during the north polar pass of the *Ulysses* spacecraft. Thus, the Spartan 201 observations were focused toward observing the north polar coronal hole of the Sun. The 42 hr of mission duration were divided into four observing sequences. The west limb of the Sun was viewed during 15:42–24:06 UT (day of year [DOY] 251), the north polar hole was viewed during 00:55–15:40 UT (DOY 252), the east limb was viewed during 16:26–21:42 UT (DOY 252), and the north pole was observed once more during 23:12–09:42 UT (DOY 252–253). The field of view of the WLC image frame and instrument details are provided in FG95.

Based on the experience of the Spartan 201-01 mission (FG95), *only pB* observations proved useful for a quantitative estimate of density in a polar coronal hole. The weak signal in coronal hole pB observations is enhanced by taking repeated pB observations for longer exposure times, which can then be co-added to increase the signal-to-noise ratio. Thus, we increased the number of polarized brightness observation sequences by a factor of 4 as compared with the previous missions.

Figure 1 (Plate L17) presents a normalized co-added image of the whole Sun by adding all long-exposure observations from the three viewing angles. This figure provides a steady state view of the solar corona. While the large-scale coronal streamers at low-to-mid latitudes show some rotational and temporal evolution, no such evolution was observed in the high-latitude polar plumes/rays, an observation made earlier by the Spartan 201-01 WLC. The image in Figure 1 was for demonstration of the WLC field of view only. To study the quantitative aspects of the steady state behavior of the north polar coronal hole, 10 image frames (composed of 30 linear polarized scans of 15.1 s exposure) during the first north polar

[1] Also Physics Department, Catholic University of America, Washington, DC.

pass (00:55–15:40 UT on September 9) of the mission were co-added. A normalized version of the north coronal hole image is presented in Figure 2 (Plate L18). The streamers in this image have been blocked out to increase the contrast between the plumes and the background coronal hole (compare with Fig. 1).

3. PHYSICAL PROPERTIES

3.1. *Polarization Brightness*

Since *pB* observations of the solar corona are related to electron density through a line-of-sight integral, observations of the coronal hole *pB* show an unavoidable overlapping of many structures along the line of sight. This makes it difficult to infer the true electron density of a coronal hole. To reduce the inherent uncertainty imposed by structures along the line of sight, the darkest region of the north polar coronal hole for a 20° angular width (position angle [P.A.] 15°–35°) was chosen. Note that Mark III K-coronameter data extend the WLC Spartan data below the edge of the orbital instruments' occulting disk. Observations of *pB* for P.A. 15°–35° as a function of height are plotted in Figure 3*a* (Plate L19). We believe that the *pB* values from the coronal hole tend to fall at the lower boundary of the range of *pB* values observed at each height. Thus, the black line in Figure 3*a* represents the lower limit of the measurable coronal hole *pB*, while the elevated values observed at any given position angle are contributions of foreground and background structures, including plumes, along the line of sight. Since even the lowest measurable *pB* measurements have contaminations from line-of-sight structures, deconvolving such data to obtain the electron density typically provides only an upper limit of the coronal hole density (Guhathakurta & Holzer 1994 and FG95). For comparison, the coronal hole *pB* profile from the first mission (FG95) is plotted as a blue line. The most significant difference between the profiles from Spartan 201-01 and 201-03 is in the level of noise reduction in the latter data. The Spartan 201-01 data showed mostly noise at great distance from the Sun. We were able to get a higher signal-to-noise ratio in the third mission by increasing the number of observations at longer exposures, especially in the outer corona. The *pB* profiles from Spartan 201-01 and 201-03 match quite well in the radial range 1.16–3.5 $R_\odot$. However, in the outer corona, the newly inferred *pB* profile is 20%–50% higher than the previous profile.

3.2. *Electron Density*

It has been shown (GHM96; Guhathakurta & Holzer 1994) that during the quiescent phase of the solar cycle, the density inside a polar coronal hole is independent of latitude and longitude and hence is a function of radial distance *r* only. Thus, the observed values of *pB* as a function of height in the coronal hole, combined with the assumption that these values vary with *r* only and with the use of the same approach as in Guhathakurta & Holzer (1994) and GHM96, permit an estimation of electron density. The density for the north polar coronal hole is plotted as a black line in Figure 3*b*. For comparison, the density inferred from Spartan 201-01 is plotted as a blue line. The variation in the two density profiles follows directly from the variation observed in the two *pB* profiles in Figure 3*a*.

The uncertainty in the electron density follows directly from the uncertainty in the *pB* data plus that from modeling. The uncertainty in *pB* depends on the height in the corona. This is the result of the weakening of the coronal signal as a function of height and also scattering of coronal light by the external occulting disk. Mark III data are most uncertain in the region 1.4–1.8 $R_\odot$, while WLC data are most uncertain in the region 1.25–1.6 $R_\odot$ because of stray light. The uncertainty in electron density in the polar region from 1.16 to 1.3 $R_\odot$ is around 15% and from 2 to 6 $R_\odot$ is 13%. The uncertainty in the region from 1.4 to 1.6 is the greatest (30%–35%), because this is where Mark III and Spartan data sets have their greatest uncertainty.

The inferred coronal hole density profile showed a variation that is inversely proportional to the square of the radial distance *r* in the outer corona. Hence, we were able to extrapolate the Spartan polar coronal hole density all the way to 1 AU and beyond, where the *Ulysses* spacecraft took in situ particle measurements. The close agreement between the extrapolated coronal hole density (*lower curve*) and *Ulysses* observations is presented in Figure 3*c*. The *Ulysses* observations include all high-speed solar wind data observed for latitudes northward of +34° in the north polar coronal hole, spanning a time frame of 1995 July 2–1996 June 25 and radial distances of 1.8–4 AU. The data were observed by the SWOOPS instrument and provided to us by D. McComas (1996, private communication). A detailed description of the data and the particles and fields experiments aboard the *Ulysses* spacecraft is provided by Bame et al. (1992). *Ulysses* particle (proton) data as a function of heliospheric distance during the spacecraft's high-latitude excursion in the north polar coronal hole are presented in Figure 3*c*.

The electron densities observed by *Ulysses*, in the fast solar wind (inside a polar coronal hole), show a variation of a factor of 1.5–2 between 1.8 and 4 AU. The data appear to be noisier beyond 3 AU. Similar variations in coronal hole *pB* observations (hence electron density) as a function of height were reported from the *Skylab* and Mauna Loa coronagraphs during 1973–1976 (GHM96) and more recently from the Spartan 201 coronagraph (FG95) and this study. Earlier observations from the Spartan 201 WLC suggested the plume density to be a factor of 1.5–2 higher than the background coronal hole (Guhathakurta & Fisher 1995 and FG95). Based on this information, the upper curve in Figure 3*c* was chosen to be a factor of 1.5 higher than the lower curve. The extrapolated upper and lower curves in Figure 3*c* provide very good limits on the range of observed *Ulysses* density variations. The large density variation in the coronal hole region in *Ulysses* observations is simply a consequence of high-density structures. However, one might speculate that since both the remote-sensing observations (Spartan *pB*) and in situ observations of the heliosphere (*Ulysses* density) show the same factor of 1.5–2 variation in the coronal hole measurements, these structures are remnants of polar plumes.

The extrapolated coronal hole density also agrees very well with the inferred density (height range of 23.5–26.5 $R_\odot$) from the ranging or time-delay measurements made during the superior conjunction of the *Ulysses* spacecraft in 1995 March (Guhathakurta, Fisher, & Woo 1996). This is the first time that an electron density profile in the coronal hole has been derived that starts at the Sun (1.15 $R_\odot$) and extends to the outer heliosphere. The empirical constraints that such a density model can provide toward solar wind modeling are discussed in the subsequent sections.

3.3. *Constraints on Solar Wind Velocity near the Sun*

Flow velocity in the coronal hole has not been directly measured. Indirect inferences of the flow velocity have been ob-

tained from Spartan and *Solar and Heliospheric Observatory* Ultraviolet Coronagraph Spectrometer (*SOHO*/UVCS) measurements using spectral line intensities as well as line widths (Strachan et al. 1997). However, spectral line intensities depend on density and temperature, while the line widths of ions are affected by the temperature of the ions, turbulence, and waves. Flow velocity in the coronal hole has also been inferred from interplanetary scintillation (IPS) measurements as close as 10 $R_\odot$ (Grall et al. 1996). But these measurements are sensitive to density fluctuations that might be influenced by waves, and thus it is difficult to unravel what the IPS signal means for the flow velocity of the protons. Flow velocity can also be inferred from the knowledge of electron density profiles out to 1 AU and particle flux measurements at 1 AU. What is also required is the knowledge of the magnetic field geometry. The following paragraph provides the basis for the calculation of flow velocity in the coronal hole, when its density is known.

A steady, one-fluid description of a proton-electron solar wind can be described by using an equation of conservation of mass flux,

$$N(s)V(s)A(s) = K, \tag{1}$$

applied along the flow tube s. The area of the flow tube is given by

$$A = A_0 f(s)\left(\frac{s}{s_0}\right)^2. \tag{2}$$

where $f(s)$ is the expansion factor or the term describing the nonradial divergence. The velocity of a particle along a flow tube can be represented as

$$V(s) = \frac{\langle N_e V_e\rangle A(s = 1\ \mathrm{AU})}{N(s)A(s)} = \frac{\langle N_e V_e\rangle f(s = 1\ \mathrm{AU})215^2}{N(s)f(s)s^2}. \tag{3}$$

A plot of the proton flux density as a function of heliospheric distance is presented in Figure 3*d*. The velocity fluctuations of the high-speed stream in the *Ulysses* data are between 5% and 15%, whereas the density can vary by a factor of 2 (Fig. 3*c*). Thus, the particle flux density $\langle NV\rangle$ shows a similar variation as the particle density. The lower curve of Figure 3*d* (similar to the lower curve in Fig. 3*c*) represents the particle flux density inside a coronal hole, which, at 1 AU, was

$$\langle N_e V_e\rangle \approx 1.5 \times 10^8\ \mathrm{cm^{-2}\ s^{-1}}. \tag{4}$$

Thus, using a known density distribution and geometry of flow tubes and ignoring the effects of solar rotation, we can infer the velocity of the solar wind from the above equations.

With accurate information on the density and particle flux, equation (3) suggests that the uncertainty of flow stream lines near the Sun is a direct function of the uncertainties in the inference of the nonradial expansion factor (eq. [2]). When estimated from the boundary of an observed polar coronal hole under the assumption that flow tubes are homologous in latitude, the maximum nonradial expansion factor was higher than 7 (Munro & Jackson 1977; Guhathakurta & Holzer 1994). An expansion factor of 2 was used in the Habbal et al. (1995) model. This difference in the expansion factor translates to a factor of 3–4 uncertainty in the estimates of the solar wind speed profile close to the Sun. We chose two different flow tube geometries: (1) the Habbal et al. (1995) divergence as a function of distance, with a peak expansion factor of 2; and (2) a flow tube geometry of the polarmost flow tube with a peak expansion factor of 9.5, obtained from a model by Guhathakurta et al. (1997, 1998) and Sittler & Guhathakurta (1997, 1998). This difference in the expansion factors translates to a factor of 4.75 uncertainty in the estimates of the solar wind speed profile close to the Sun. If we choose just a radial geometry, the uncertainty is 9.5. The two different flow tube expansion factors are presented in Figure 4*a* (Plate L20). Computed velocities are plotted in Figure 4*b* as a function of the heliospheric distance, 1–215 $R_\odot$, for the two respective flow tube expansion factors of Figure 4*a*. All other parameters being equal, the velocity is directly proportional to the maximum expansion factor of the flow tube. Also plotted in Figure 4*b* is the continuous profile of the electron density (*black line*). The velocity (*red line*) inferred from the current density profile and the expansion factor given by the red line in Figure 4*a* are in very good agreement with the *Ulysses* measurements of the high-speed polar wind. The green line is the inferred velocity using the Habbal et al. expansion factor, which shows a similar value as our model in the region where the flow tube divergence becomes radial but is significantly different in the inner corona. The velocity estimated from our density model, close to the Sun, seems to be in the same range as the current interpretations of velocities inferred from *SOHO*/UVCS observations (Strachan et al. 1997).

3.4. *Effective Coronal Temperature*

Recent results from *SOHO*/UVCS suggest that the protons are much hotter than the electrons in the inner/outer corona. In this context, the effectiveness of a single-fluid solar wind model has been questioned. In this section, we present calculations to show that, from coronal density alone, we can determine an effective temperature of the corona that can provide constraints on observed or modeled temperatures in the corona.

The single-fluid solution of the hydrostatic equation can be written as

$$\frac{dP}{dr} = \frac{M_\odot G\rho}{r^2}, \tag{5}$$

where, for an ideal gas, the pressure is given by $P = NkT$, where N is the total number of particles per unit volume and k is the Boltzmann constant. The density can be specified in terms of a mean atomic weight μ, which essentially is the average mass per particle in units of proton mass m_{H}, where

$$\rho = \mu m_{\mathrm{H}} N, \quad P = \frac{k}{\mu m_{\mathrm{H}}}\rho T. \tag{6}$$

For a gas composed of fully ionized hydrogen, μ is 0.5, whereas μ is 0.62 for a fully ionized mixture having a hydrogen-to-helium number density ratio of 9 to 1 with a helium fraction of $\alpha = 1$. Using the above equations, and assuming the gas to be locally isothermal, and since the total density distribution is the same as the electron density distribution scaled by a constant factor (Guhathakurta & Fisher 1995), we get

$$\frac{N(r)}{N(R_\odot)} = \exp\left[-\frac{\mu m_{\mathrm{H}} g_\odot R_\odot}{kT}\left(1 - \frac{R_\odot}{r}\right)\right], \tag{7}$$

where $g_\odot$ is the value of solar gravity at $r = R_\odot$. For a two-fluid gas, $N = N_e + N_p = 2N_e$ and $P = N_e kT_e + N_p kT_p = 2N_e k(T_e + T_p)/2$. Equation (7) can be written as

$$\frac{N(r)}{N(R_\odot)} = \exp\left[-\frac{\mu m_{\rm H} g_\odot R_\odot}{k(T_e + T_p)/2}\left(1 - \frac{R_\odot}{r}\right)\right]. \quad (8)$$

Thus, in the context of the two-fluid solution, the scale height temperature becomes an effective temperature, such that $T = (T_e + T_p)/2$. If we have an estimate of either T_e or T_p from either observations or models, the other parameter can be computed from T. One such example is provided by choosing T_e and T_p from the Habbal et al. (1995) two-fluid model. The average temperature of T_e and T_p from this model is plotted in Figure 5 (Plate L20). We find that the average temperature agrees very well ($\pm 15\%$) with our temperature computed from density. For comparison, T from the 1993 flight is also plotted in Figure 5, and it does not agree very well with the Habbal et al. (1995) model. The difference in the two profiles is a direct consequence of the inference of a more accurate density profile in the outer corona from the Spartan 201-03 mission.

Since the electron density is analytically prescribed as a function or r, T can be derived without assuming an isothermal condition. If ρ is known as a function of r, then P can be obtained as a function of r by integrating equation (5). Once P is known, T can be directly computed ($T = P/NK$), and there is only a 10% difference with temperature T, estimated by assuming hydrostatic and locally isothermal conditions. Thus, the original assumption of the corona being locally isothermal appears justified. In the multifluid context, T is simply

$$\mu \frac{1 + 2\alpha}{1 + 4\alpha} \frac{P}{Nk}$$

(see Gibson et al. 1998).

Determination of coronal temperature in this way rests on two assumptions: (i) Equation (6) has been derived from a complete momentum balance on the gas by assuming $\boldsymbol{V}$, the macroscopic velocity, to be zero (hydrostatic atmosphere), which makes our derived values of temperature a lower bound. Recent calculations of temperature under hydrodynamic conditions have been presented by Sittler & Guhathakurta (1998). (ii) We have also neglected the Lorentz force ($\boldsymbol{J} \times \boldsymbol{B}$, where $\boldsymbol{J}$ is the electric current density), which is valid in the coronal hole and outer corona. When the $\boldsymbol{J} \times \boldsymbol{B}$ force is nonnegligible, equation (7) is still valid for the component parallel to the field.

4. SUMMARY

Polarized observations of the corona in the range 1–6 $R_\odot$ offer the *cleanest* measurement for quantitative studies of the corona since these observations depend only on the density along the line of sight. This Letter demonstrates the importance of white-light *pB* observations for inferring the electron density in the coronal hole and the key role played by this parameter in providing empirical constraints on solar wind structure, especially near the Sun.

The principal findings of the Spartan 201-03 WLC observations of the polar corona and *Ulysses* observations of the high-latitude solar wind as reported in this Letter are as follows:

1. We were able to combine in situ and path-integrated measurements to yield a consistent electron density profile from the Sun to the Earth and the outer heliosphere in the polar coronal hole. The extrapolated Spartan coronal hole density profile agreed very well with the *Ulysses* in situ observations. Thus, by using the in situ value of N measured by *Ulysses* (1.8–4 AU), we were able to determine the actual value of the N profile and *not just an upper limit* in the polar coronal hole, near the Sun.
2. Interpreting IPS observations, Grall et al. (1996) suggested that the solar wind was accelerated by 12 $R_\odot$. However, the interpretation of IPS observations close to the Sun remains a difficult task. The current N profile suggests that the acceleration of the solar wind is almost complete by 10–15 $R_\odot$.
3. A meaningful effective temperature of the corona can be inferred from the knowledge of the gradient of density only.
4. With accurate information on the density and particle flux, equation (3) suggests that the uncertainty of flow stream lines near the Sun is a direct function of the uncertainties in the inference of the magnetic geometry of flow tubes.

The authors gratefully acknowledge the engineering support of the White-Light Coronagraph instrument, provided by Greg Card and Judd Johnson. We appreciate the support of A. Hundhausen, Alice Lecenski, and Joan Burkpile for kindly providing the Mark III K-coronameter data and Dave McComas for providing the *Ulysses* data used in the study. The present work was supported by a grant from the NASA suborbital research program of the Space Physics Division and a NASA grant (5-2881) to the Catholic University of America.

REFERENCES

Allen, C. W. 1973, Astrophysical Quantities (Oxford: Athlone)
Bame, S. J., McComas, D. J., Barraclough, J. L., Phillips, K. J., Sofaly, J. C., Chavez, J. C., Goldstein, B. E., & Sakurai, R. K. 1992, Ap&SS, 92, 237
Fisher, R., & Guhathakurta, M. 1995, ApJ, 447, L139 (FG95)
Gibson, S. E., Fludra, A., Bagenal, F., Biesecker, D., Del Zanna, G., & Bormage, B. 1998, J. Geophys. Res., submitted
Guhathakurta, M., & Fisher, R. R. 1995, Geophys. Res. Lett., 22(14), 1851
Guhathakurta, M., & Fisher, R. R. 1996, in AIP Conf. Proc. 385, Robotic Exploration Close to the Sun: Scientific Basis, ed. S. R. Habbal (New York: AIP), 121
Guhathakurta, M., Fisher, R., Sittler, E. C., Roberts, A., McComas, D., Zhao, X., & Hoeksema, T. 1997, Eos: Trans. AGU, 78(17), S253
Guhathakurta, Fisher, R. R., & Woo, R. 1996, Eos: Trans. AGU, 77(46), F586
Guhathakurta, M., & Holzer, T. E. 1994, ApJ, 426, L782
Guhathakurta, M., Holzer, T. E., & MacQueen, R. M. 1996, ApJ, 458, 817 (GHM96)
Guhathakurta, M., Sittler, E. C., Fisher, R. R., McComas, D., & Thompson, B. 1998, in preparation
Grall, R. R., Coles, W. A., Klinglesmith, M. T., Breen, A. R., Williams, P. J. S., Markkanen, J., & Esser, R. 1996, Nature, 379, 429
Habbal, S. R., Esser, R., Guhathakurta, M., & Fisher, R. R. 1995, Geophys. Res. Lett., 22(12), 1465
Ko, Y.-K., Lennard, F. A., Geiss, J., Gloeckler, G., Galvin, A. B., & Guhathakurta, M. 1997, Sol. Phys., 171, 345
Munro, R., & Jackson, B. V. 1977, ApJ, 213, 874
Sittler, E. C., & Guhathakurta, M. 1997, Eos: Trans. AGU, 78(17), S255
———. 1998, ApJ, submitted
Strachan, L., et al. 1997, in Proc. Fifth *SOHO* Workshop, The Corona and Solar Wind near Minimum Activity (SP-404) (Noordwijk: ESA), 691

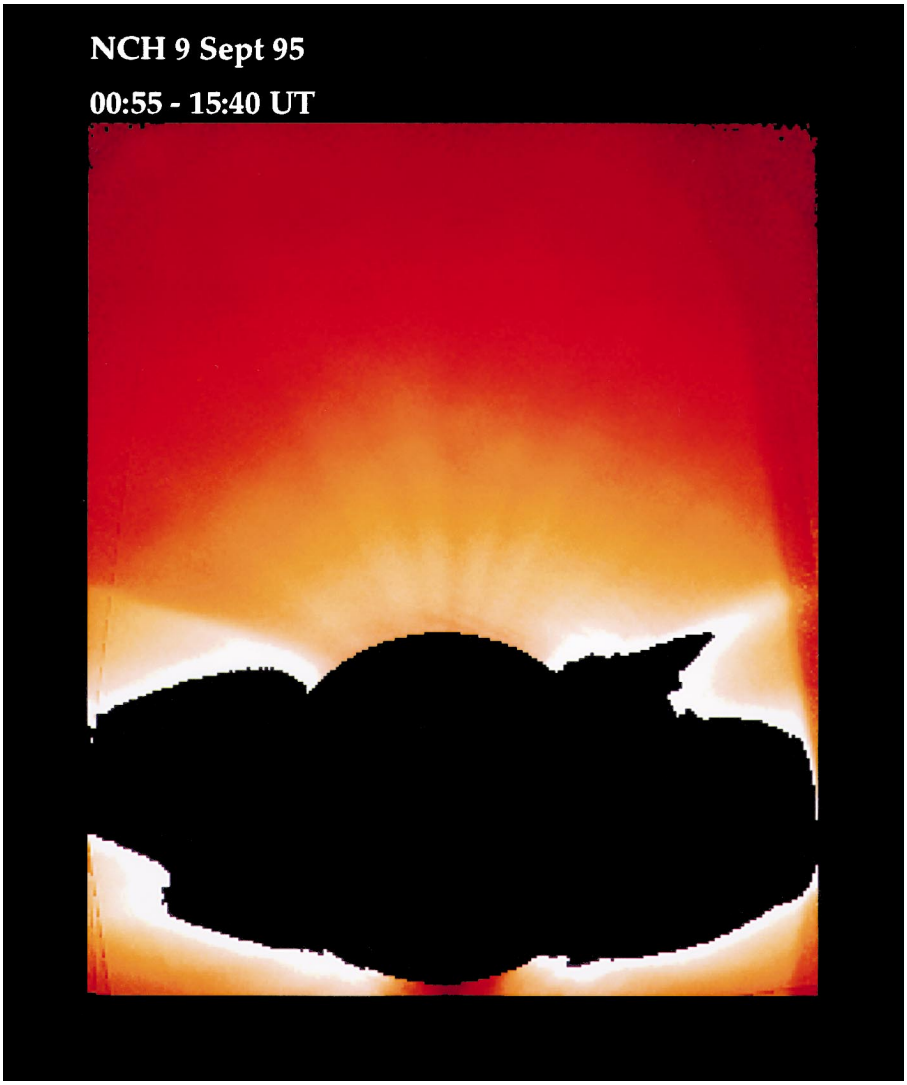

FIG. 1.—A mosaic of the *pB* image of the corona encompassing the different fields of view for 1995 September 8–10 representing the steady state corona from 1.6 to 6 $R_{\odot}$. The inner image is from the ground-based Mark III coronagraph from 1.15 to 1.4 $R_{\odot}$.

GUHATHAKURTA & FISHER (see 499, L215)

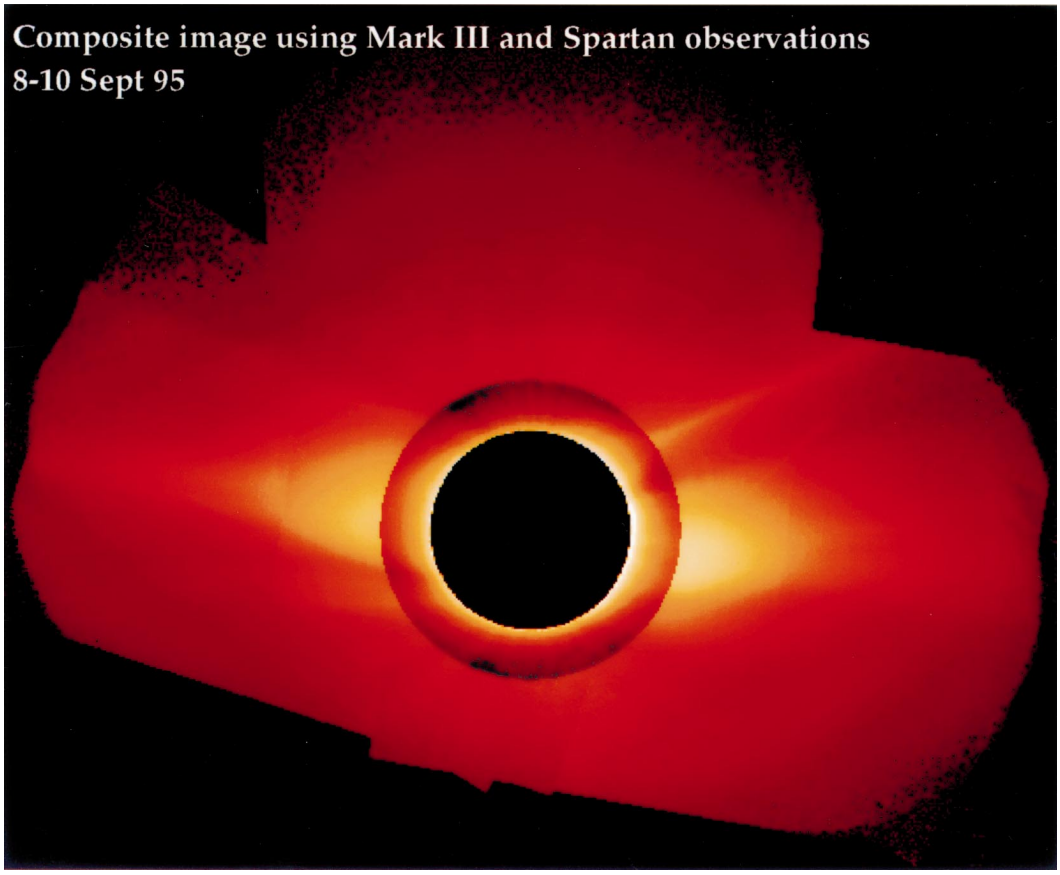

FIG. 2.—Image of the north polar coronal hole. The streamers are masked to enhance the contrast between the plumes and the coronal hole.

GUHATHAKURTA & FISHER (see 499, L216)

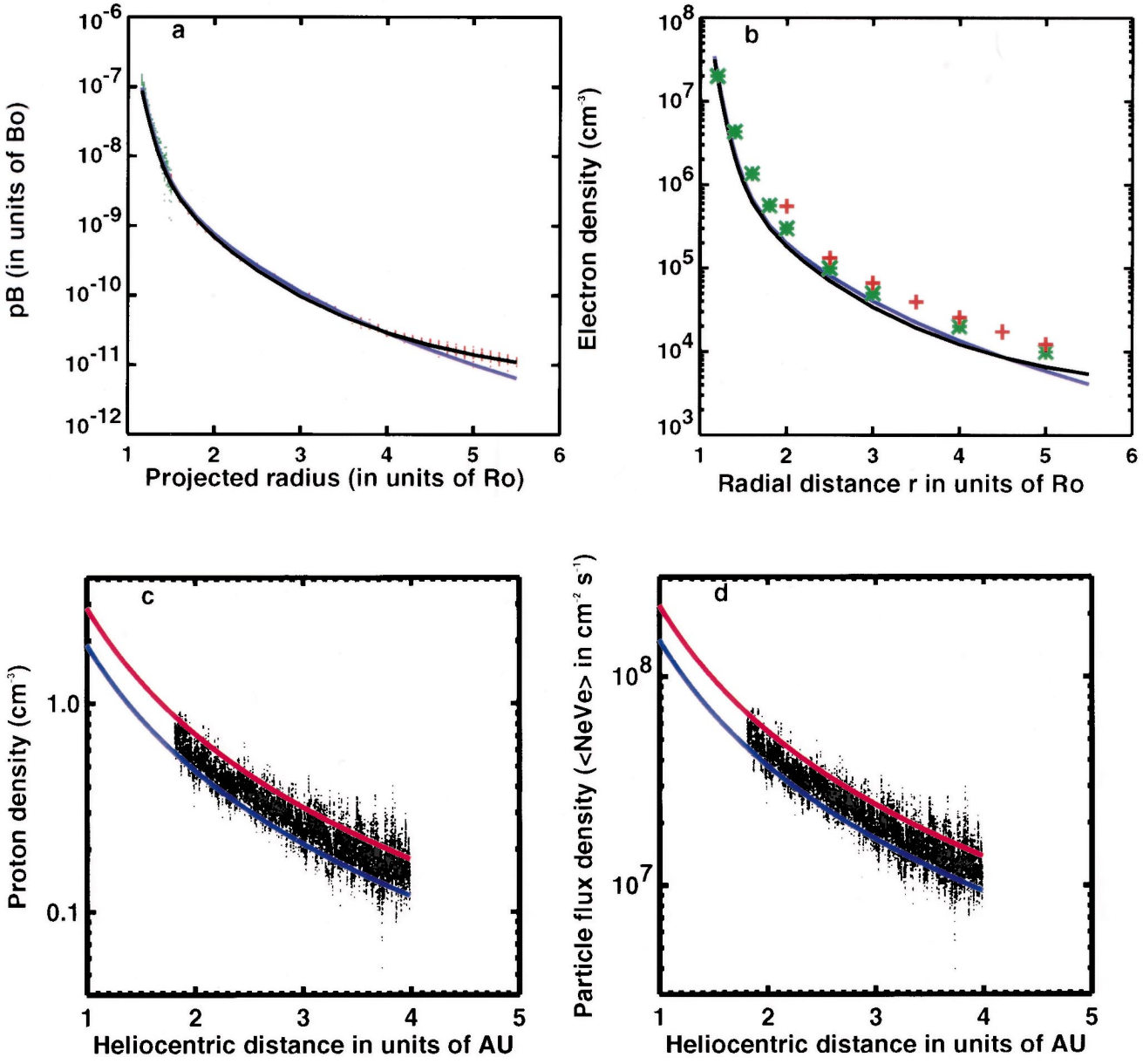

FIG. 3.—(*a*) Estimates of *pB* data in the 20° angular bin from Spartan 201-03 and the Mark III coronagraph for the north pole at P.A. 15°–35°. The green dots represent Mark III observations from 1.16 to 1.5 $R_{\odot}$, while the red dots are from the Spartan WLC from 1.5 to 5.5 $R_{\odot}$. The black line is the current fit to the coronal hole *pB* data, while the blue line is from Spartan 201-01. (*b*) Estimated density for the north polar coronal hole as a function of the radial distance. The black and blue lines represent the north coronal hole for the 1995 and 1993 electron densities, respectively. The crosses are for the Munro & Jackson (1977) polar value, and the asterisks are for the Allen (1973) minimum polar value. (*c*) The *Ulysses* proton density as a function of heliocentric distance from 1.8 to 4 AU for latitudes upward of 34° in the north polar coronal hole. (*d*) The *Ulysses* proton flux density for the same data as in (*c*).

GUHATHAKURTA & FISHER (see 499, L216)

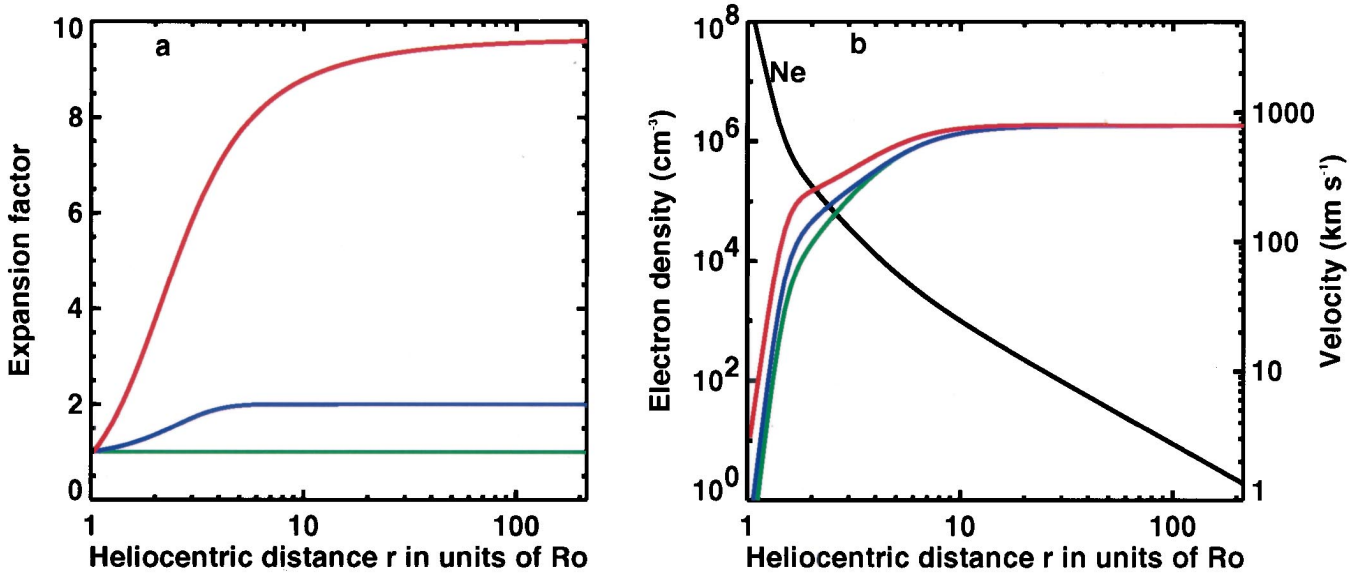

FIG. 4.—(*a*) The red line is the expansion factor of the polarmost flow tube obtained from the Guhathakurta et al. (1997) model. The blue line is the expansion factor used in the Habbal et al. (1995) model, while the green line is the expansion factor for a purely radial geometry. (*b*) The red line is the inferred velocity using the expansion factor from the Guhathakurta et al. (1997) flow tube, the blue line is that obtained using the Habbal et al. (1995) flow tube model, while the green line is for radial geometry. The black line represents the electron density from 1 to 215 $R_{\odot}$.

GUHATHAKURTA & FISHER (see 499, L217)

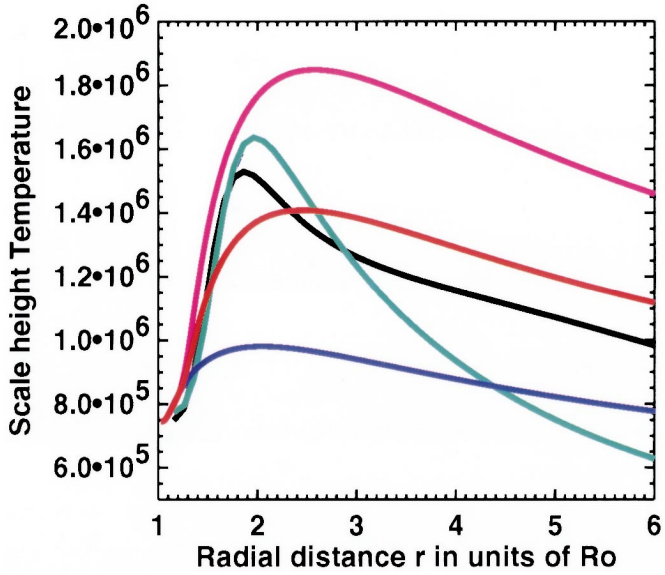

FIG. 5.—The black and green lines are the variations in coronal effective temperature T for the north coronal hole as a function of the radial distance for the 1995 and 1993 flights, respectively. The magenta and blue lines, respectively, represent proton temperature T_p and electron temperature T_e obtained from the Habbal et al. (1995) model. The red line is the average, which is equal to $(T_e + T_p)/2$.

GUHATHAKURTA & FISHER (see 499, L218)